Electronic Journal of Structural Engineering

Original Article

Cite this: DOI:10.56748/ejse.25680

Received Date: 03 September 2024
Accepted Date: 16 March 2025

1443-9255
https://ejsei.com/ejse

Mechanical Properties of Fewer-Girder Steel Plate Composite Bridges during Construction

Bo Wang [a], Rui Zuo [b*], Liang Chen [b], Wenhai Zhu [a], Yuhang Hou [a]

[a] Anhui Province Transportation Holding Group Co, Construction Management Company Limited, Hefei 230000, China
[b] School of Civil and Hydraulic Engineering, Hefei University of Technology, Hefei 230009, China
*Corresponding author: ruiliu012@yeah.net

Abstract

Composite steel plate girder bridges have become an important choice in contemporary bridge construction due to their distinctive structural features and benefits. However, stability, particularly deflection, torsion and buckling, continues to pose substantial challenges. This study aims to elucidate the structural behavior, load distribution and stress responses of such bridge designs, so as to optimize construction efficiency and ensure structural safety. To achieve these objectives, a comprehensive series of finite element analyses are conducted, focusing on the stress distribution and local stability of composite steel plate girder bridges under different construction conditions. The study emphasizes that the 2nd and 4th piers, as well as the mid-span of the edge spans, are particularly sensitive to concentrated stress and potential local buckling. The findings indicate that composite steel plate girder bridges with a reduced number of main girders have significant mechanical properties compared to traditional designs. Specifically, the reduction in the number of main girders will affect the load distribution and stress concentration mode, which have a significant impact on the construction process and long-term performance of the bridge.

Keywords

Composite steel plate girder bridge, Mechanical performance, Stability, Finite element, Bridge construction

1. Introduction

As an important component of modern transportation infrastructure, bridges have attracted great attention in engineering and academia. Due to the advancement of engineering technology and the rapid growth of transportation demand, the design and stability of bridge structures have become increasingly important (He et al., 2023). Steel plate composite girder bridges have become a mainstream choice in contemporary construction due to their unique structural characteristics and advantages.

Steel plate composite girder bridges combine the high strength of steel and the stability of concrete, providing excellent load-carrying capacity, seismic resistance, and durability (Wei et al., 2021). This structural form is known for its fast construction, economic efficiency, and adaptability, making it particularly suitable for large-span and complex terrain bridge projects (Li et al., 2022). However, challenges such as flexure, torsion and buckling can pose stability issues, leading to structural failures and compromising bridge safety (Kaplan et al., 2021; Zhou et al., 2020; Ding et al., 2021; He et al., 2022).

Jiang et al. (2021) emphasized the importance of considering multiple hazards in stability analysis, taking into account various environmental and load conditions in construction. Liang et al. (2022) introduced a staggered-supported steel anchor box system for cable-stayed bridges, demonstrating the advancement of anchoring techniques to improve stability. Xu et al. (2022) explored the mechanical behavior of a new steel-concrete joint in hybrid continuous bridges, deepening our understanding of joint performance under construction loads. Rossi et al. (2020) evaluated the transverse torsional buckling in steel-concrete composite beams, which is critical for preventing structural failures. Soto et al. (2020) provided empirical data on the performance of steel concrete composite box girders under bending, shear, and torsion. Csillag and Pavlović (2021) studied the push-out behavior of demountable connectors in FRP decks, offering insights into connector performance in the assembly stage. He et al. (2022) and Jung et al. (2022) tested a locking-bolt demountable shear connector to enhance the understanding of connector behavior under construction loads. Bajaber and Hakeem (2021) and Chithra et al. (2022) developed demountable bolted shear connectors for modular constructionto emphasize the importance of ease in deconstruction and reconstruction. Lee et al. (2021), Biscaya et al. (2021) and Siwowski et al. (2021) reviewed the application of Ultra-High-Performance Concrete (UHPC) in construction to improve the mechanical performance of composite girder bridges.

Even this, there is still a gap in understanding the mechanical properties of composite girder bridges with fewer main girders during construction. This study focuses on the mechanical behavior and stability of composite steel plate girder bridges with reduced main girder configurations during construction. Most literatures mainly emphasize traditional configurations with standard numbers of main girders, exploring aspects such as load distribution, seismic resistance, and long-term durability. However, there is limited understanding of how fewer main girders impact the structural performance in main construction phases. Based on a series of comprehensive finite element simulations and experimental validations, this study elucidates the effects of reduced girder configurations on stress distribution, deflection patterns, and local instability. The findings are of great significance for optimizing design and improving bridge construction safety, especially under challenging terrain and loading conditions.

2. Material and Methods

The upper structure of the main bridge is designed with a double I-beam steel plate, with a total width of 25.5 m on both sides. The steel main girders use Q345qD I-beam straight web girders, with a spacing of 6.7 m and a height of 1.8 m. Concrete deck slabs are connected to the steel girders using clustered welding nails, and bolted crossbeams are used between the main girders to enhance lateral connection. The smaller crossbeams are spaced 7.0 m and reduced to 3.5 m at the pivot point. Prefabricated bridge deck panels are longitudinally connected through reinforced concrete wet joints and fully prefabricated horizontally through transverse pre-stressing to improve structural integrity. There are pre-drilled holes on the bridge deck slabs, and shear nails at the top flange and wet joint of the steel girders. Once the deck slabs are in place, wet joints and shear channel concrete are poured to connect them to the steel girders. The 35 m standard span deck slabs are divided into three types: 3.0 m standard section slabs, 3.0 m center pivot section slabs, and 3.2 m end section slabs. The width of the deck slab is 12.25 m; the thickness at the bearings, at the cantilever, and in the middle of the span is 0.4m, 0.22m, and 0.257m, respectively. The longitudinal reinforcement at the wet joints is overlapped in a ring manner, as shown in Figs. 1-2.

2.1 Finite element modeling

A baseline model consisting of a continuous girder with a span combination of 4×25 m is established. A refined finite element analysis model of the main girder is developed using ABAQUS. As shown in Fig. 4, the concrete slab is modeled using C3D8R elements, the steel main beam using S4R shell elements, and the steel reinforcement using T3D2 elements. The reinforcement is embedded within the concrete elements. Binding constraints are applied between the concrete and steel main beam elements at corresponding positions in the baseline model.

Fig. 3 shows a completely symmetrical support arrangement under self-weight, where W1-W3 (collectively referred to as Support 1, Support 2, etc.) is used to analyze mechanical properties.

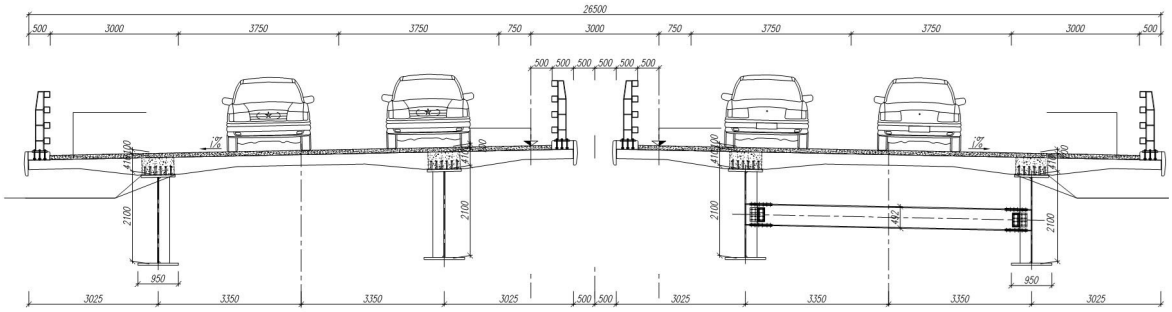

Fig. 1 Layout of the steel plate combined girder bridge section

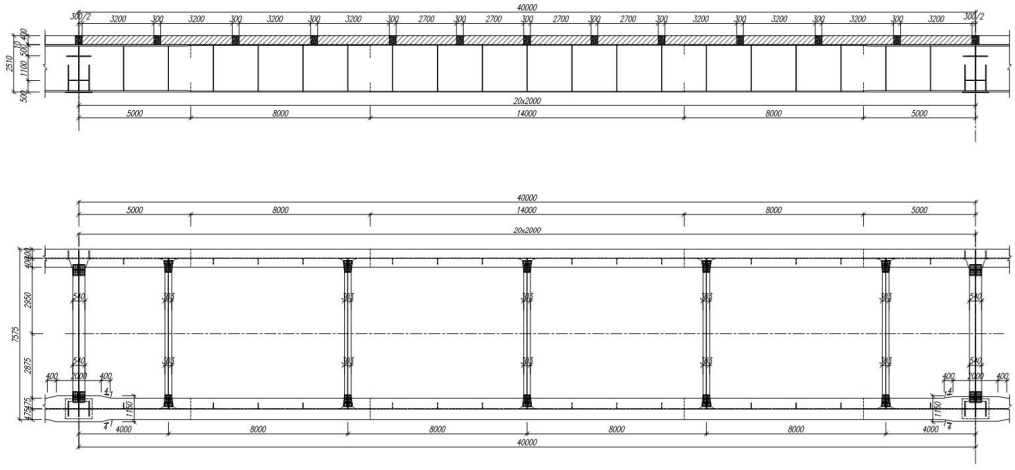

Fig. 2 Layout of the steel plate composite girder bridge

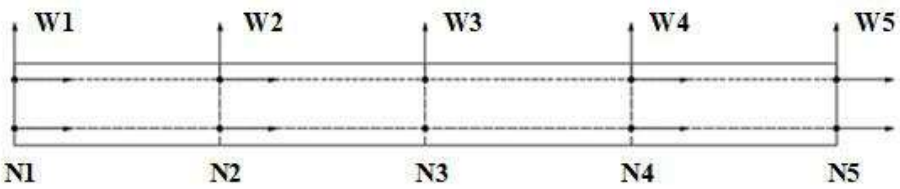

Fig. 3 Support arrangement diagram

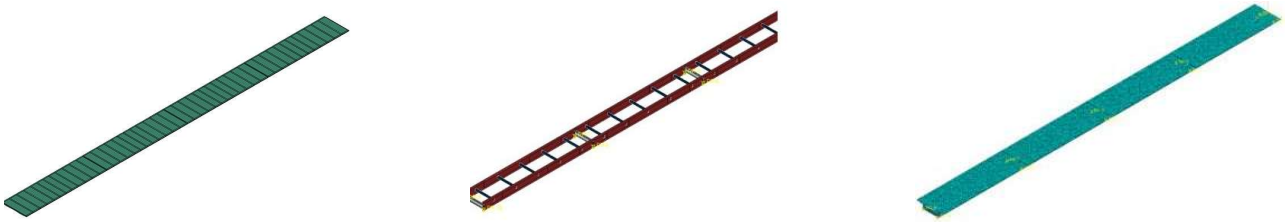

(a) Upper concrete slab (b) Lower steel main girder and crossbeam (c) Meshing

Fig. 4 Schematic diagram of finite element model

The stress-strain curve in the concrete compression stage is determined according to the GB50010-2010 code.

$$\sigma_c = \begin{cases} \frac{\rho_c n}{n-1+x^n} E_c \varepsilon_c & x \le 1 \\ \frac{\rho_c}{\alpha_c (x-1)^2 + x} E_c \varepsilon_c & x > 1 \end{cases} \quad (1)$$

$$\rho_c = \frac{f_c}{E_c \varepsilon_{cr}} \quad (2)$$

$$n = \frac{E \varepsilon_{cr}}{E_c \varepsilon_{cr} - f_c} \quad (3)$$

Where σ_c represents the compressive stress of the concrete; ε_c Denotes the compressive strain of the concrete; ε_{cr} is the uniaxial compressive strength of the concrete cube; f_c is the corresponding peak compressive strain of the concrete, and α_c is the parameter of the descending segment of the uniaxial compressive stress-strain curve, which controls the rate of strength degradation after the peak. The larger α_c, the faster the concrete strength declines. $0.157 f_{cu}{}^{0.785} - 0.905$ and the expression is$x = \varepsilon_c / \varepsilon_{cr}$.

To accurately simulate the construction process of the composite steel plate girder bridge, the 'birth-death element' method is used in the finite element model. This method allows the sequential activation and deactivation of elements to represent actual construction sequence. At each stage, the elements corresponding to newly installed components such as girders and deck slabs are activated, while the components that have not yet been constructed remained inactive. This method ensures that stress distribution and structural behavior at each stage are accurately represented. The modelling process incorporates all 13 construction phases listed in Table 1 and adds or modifies elements based on specific construction operations. Mechanical property and local instability analysis is conducted on a benchmark bridge to determine the most unfavorable construction conditions and the most vulnerable instability locations. This study examined the stress distribution of steel plate composite girder bridges under different construction scenarios.

3. Results and analysis

For mountainous highways, the application of steel plate composite girders is limited by transportation routes and terrain conditions, making the installation of steel girders particularly challenging, especially in river crossings, road crossings, and uneven terrains. To address these problems, reinforcing large-scale bridge erection machinery and modifying outrigger force pivot points can optimize the process, enabling steel plate composite girders to be erected on different pier widths. In addition, the strategy of delaying the erection of bridge decks after the installation of each span of steel girders provides continuity, convenience, economy, and efficiency in construction. The construction process of a four-span, single-link steel plate composite girder bridge is divided into 13 phases, as shown in Table 1. Table 1 provides the construction process of steel plate composite

girder bridge, including 13 sequential phases from S1 to S13. The process first installs the steel girder for span 1 (S1), then installs the steel girder for span 2, and welds the girders from spans 1 and 2 (S2). In S3, the bridge deck for span 1 is spliced to establish continuity, and in S4, the wet joint of span 1 is poured to ensure structural integrity. The steel girder of span 3 is installed in S5, and the girders of spans 2 and 3 are welded together. This is followed by the splicing of deck slabs of span 2 (S6) and the pouring of the wet joint of span 2 (S7). In S8, the steel girders of span 4 are installed and the girders of spans 3 and 4 are welded, followed by the splicing of deck slabs of span 3 in S9 and the pouring of the wet joint of span 3 in S10. The process continues with the splicing of deck slabs of span 4 in S11, the pouring of the wet joint of span 4 in S12 and completing the construction of the bridge deck and parapets in S13, known as Phase II loading. This systematic phased approach ensures careful assembly of the bridge and provides a foundation for analyzing the structural behavior and stability at each critical stage.

Table 1. Construction of steel plate composite girder bridge

Construction phases	Construction processes
S1	Installation of span 1 steel girder
S2	Installation of 2nd span steel girder and welding of 1st and 2nd span steel girders
S3	Splicing of span 1 bridge deck
S4	Pouring the 1st span wet joint
S5	Installation of 3rd span steel girder and welding of 2nd and 3rd span steel girders
S6	Splicing of span 2 deck slabs
S7	Pouring 2nd span wet joint
S8	Installation of steel girders on span 4 and welding of steel girders on spans 3 and 4
S9	Splicing of span 3 deck slab
S10	Pouring the 3rd span wet joint
S11	Splicing of span 4 deck slab
S12	Pouring span 4 wet joint
S13	Construction of bridge decking and parapets (phase II loading)

3.1 Analysis of structural mechanical properties during construction

In the design of steel and modular structures, there are two key issues: strength and stability. On one hand, strength involves stress analysis to determine whether the maximum stress caused by the load on a single component or the entire structure exceeds the ultimate strength of the material in a stable equilibrium state. On the other hand, stability involves identifying unstable equilibrium states, in which the structure may lose its initial equilibrium and undergo uncontrollable deformation, potentially compromising its functionality. The study analyzes the mechanical properties such as deformation and stress of 13 detailed construction stages of a double main girder steel plate composite girder to determine the most unfavorable construction stages.

3.2 Stress and displacement analysis for each construction stage

Fig. 5 shows the tensile stress, compressive stress, and deflection values of the bridge at different construction stages. These values underwent significant changes before stage S13 (construction of the bridge deck pavement and parapet), particularly in stage S3 (installation of the first span deck slab) and stage S4 (pouring of the first span wet joint). In stage S4, the maximum compressive stress is at the upper flange of the mid-span of the first-span steel girder, reaching 135.72 MPa. This stress level remained relatively stable between 134.71 and 135.79 MPa until stage S12, indicating minimal changes due to subsequent construction activities. Before installing the deck slab to span 2, the maximum tensile stress is at the lower flange of the steel girder of span 1. After the installation of the deck slab of span 2, the maximum tensile stress transfers to the upper flange of pier 2. In the later construction stages, it fluctuates between the upper flanges of piers 2 and 4, ranging from 101.24 to 117.96 MPa. In stage S12 (post-pouring of the 4th span wet joint), it reaches a peak of 117.96 MPa. Throughout the construction, the deflection consistently reaches its peak at the mid-span of the first steel girder. After installing the second span deck slab, the deflection slightly decreases, ranging from 54.66 to 65.75 mm between the stages S4 and S12, and reaching its maximum in the stage S5 (installation of the 3rd span steel girder and welding of the 2nd and 3rd span girders). In stage S13, the paving layer and the self-weight of the parapet increases the overall stress. It is worth noting that at this stage, the location of the maximum compressive stress shifts from the upper flange of the side span to the top of pier 4. The most sensitive locations throughout the construction process are pier 2, pier 4, and the center of the side span. Special attention should be paid to these areas during construction to ensure structural integrity and safety.

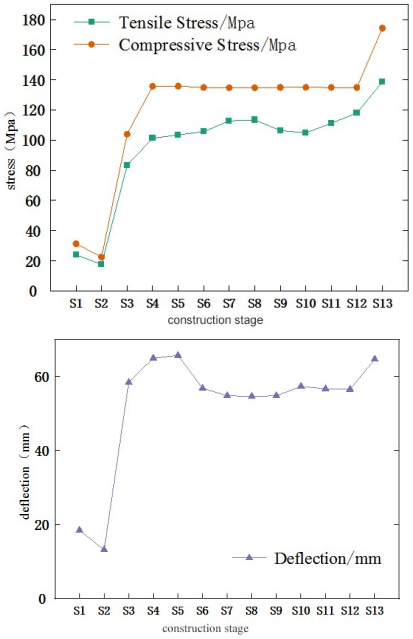

Fig. 5 Stage value comparison by stage

Based on the calculation analysis, the working conditions S3 (installation of the first span deck slab), S6 (installation of the second span deck slab), S9 (installation of the third span deck slab), and S13 (construction of the bridge deck pavement and parapet) are selected for local stress and stability analysis. These stages are characterized by the installation of deck slabs that have not yet bonded to the steel girders, resulting in insufficient constraint of the deck slab on the deformation of the steel girder. This lack of restraint may lead to excessive local stress and local buckling instability. Comparative analysis of the mechanical properties at each construction stage indicates that installing the deck slabs can significantly impact the stress and deflection of the steel main girder. Continuously changing the thickness of the upper and lower flanges and the web of the I-girder can increase the likelihood of excessive local stresses and local buckling instability. To ensure construction safety in the S13 construction stage, it is important to verify that the maximum stress of the steel plate composite beam during the secondary loading stage does not exceed the stress limit. This precaution will help maintain the structural integrity and safety of the construction process.

Local stress analysis of stage S3

Fig. 6 shows the equivalent stress cloud diagram of the combined girder bridge in stage S3. According to Fig. 6(a), before pouring the wet joints, the stress is relatively high in the upper flange area of the bridge deck slab and steel main girder is relatively high, not in contact with the bridge deck slab and the maximum stress occurs at mid-span. The highest stress recorded at 82.5 MPa in the web is concentrated at the upper end. Compared with the flange, the thickness of the web is small, which may lead to local stability losses.

In addition, stress concentrations are observed at the point where the thickness of the lower flange of the steel main beam changed. However, the overall stress in these areas is lower than it of the upper flange. Therefore, in stage S3, particular attention should be given to the junction of the upper flange and web at the mid-span of the first steel main girder span, as this area is most susceptible to instability and stress-related problems.

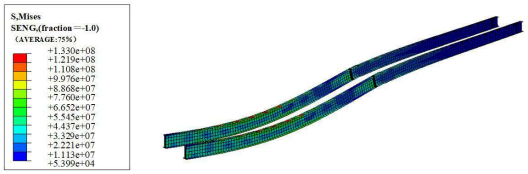

(a) Overall stress map

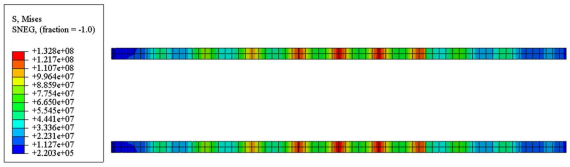

(b) Localized stress cloud at mid-span upper flange

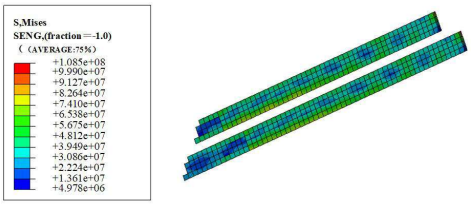

(c) Localized stress cloud in mid-span web

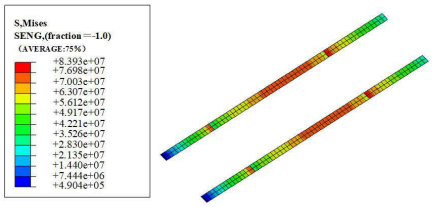

(d) Localized stress cloud at lower flange in mid-span

Fig. 6 Equivalent stress cloud of combined girder bridge under S3 stage

Localized stress analysis of stage S6

As shown in Fig. 7, the stress on the upper flange of pier 2 increases significantly after the installation of the deck slab span 2, reaching 112.0 MPa. The stress on the web is most concentrated near the lower flange of pier 2, similar to stage S3. The thickness of the web is less than that of the flange, which has raised concerns about potential local instability in this area.

The lower flange stress in the steel main girder is mainly located in three areas: the mid-span of the side span, the junctions where flange thickness changes, and the top of the pier. However, these stresses are generally lower than those in the upper flange. Under stage S6, special attention should be given to the mid-span upper flange of the first span steel main girder and the junction between the web plate and lower flange of pier 2, as these areas are critical for ensuring structural stability and integrity of the bridge.

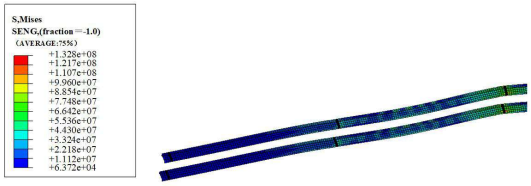

(a) Overall stress map

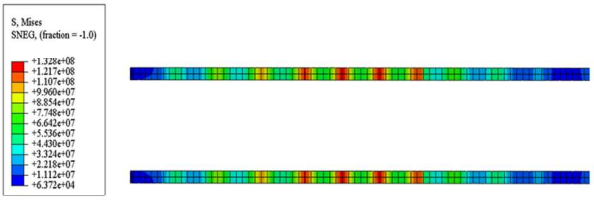

(b) Localized stress cloud at mid-span upper flange

(c) Localized stress cloud in mid-span web

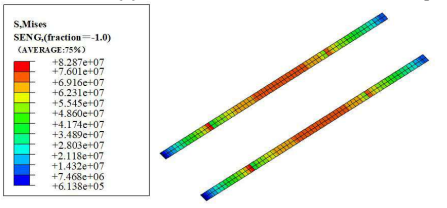

(d) Localized stress cloud at lower flange in mid-span

Fig. 7 S6 Equivalent stress cloud of combined girder bridge under stage S6

Local stress analysis of stage S9

Stage S9 has lower changes than S6. In S9, the installation of the double main girder steel plate composite girder deck slabs mainly affects the internal forces of adjacent span steel main girders, while the impact on the middle span main girders can be negligible. For the double main girder steel plate composite girder structure, with a span of four spans and one connecting rod, the most dangerous locations are concentrated around the side spans (especially the first span steel main girder) and piers 2 and 4. Consequently, the construction of the 3rd span steel main girder ranks the last in the maximum value of the overall internal force. After comparing Figs. 7(a)-(d) and Figs. 8(a)-(d), there are little differences in the maxima stress between stages S6 and S9, and the variation in Mises stresses outside the hazardous locations is less than 2 MPa. This analysis indicates that the stress distribution pattern of S9 during the construction is similar toS6, and there is no significant increase in structural risk or stress.

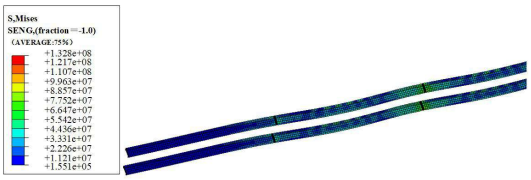

(a) Overall stress map

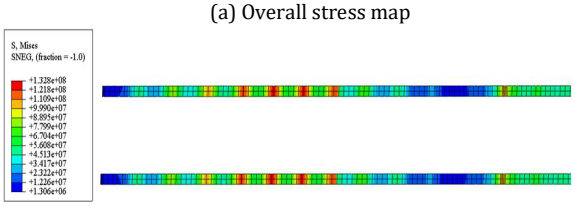

(b) Localized stress cloud at mid-span upper flange

(c) Localized stress cloud in mid-span web

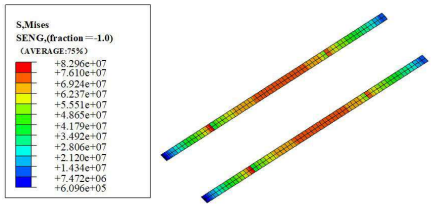

(d) Localized stress cloud at lower flange in mid-span

Fig. 8 Equivalent stress cloud of combined girder bridge under stage S9

Localized stress analysis of stage S13

After applying the second-phase loading, the stress extremum in the steel main girder shifted to piers 2 and 4. The maximum Mises stress is particularly concentrated on the web plate near the lower flange of Pier 4. The analysis indicates that under several dangerous construction conditions, the stress concentration in the double-main girder steel plate composite girders did not exceed the specified stress limits, ensuring that the girder stresses remained within a safe range. As shown in Fig. 9, the stress concentration areas are mainly located at the mid-span of the first span of the steel main girder and around piers 2 and 4. These findings emphasize the importance of monitoring these critical areas during construction to maintain structural integrity and safety.

3.3 Local stability analysis

This section addresses the stability issue of key unstable points by considering the effects of initial defects (such as geometric defects and residual stresses) as well as material and geometric nonlinearity on structural components. Initial geometric imperfections, including initial eccentricity and bending, will generate second-order moments under pressure. Material nonlinearity would result in a plastic stage after yielding, changing the load-deformation relationship to a nonlinear pattern. Residual stress will reduce the flexural stiffness of the component, prompting earlier entry into the plastic stage, thereby reducing the critical buckling load. Geometric nonlinearity, also known as large deflection theory, can cause the stiffness matrix of components to constantly change with displacement, requiring continuous adjustment of the overall structural stiffness matrix in finite element calculations.

As these factors play and the load increases, the overall stiffness of the compressed component decreases. This decline continues until the stiffness matrix of the structure becomes singular, indicating the ultimate load capacity of components. Beyond this point, even without increasing additional load, the deformation of the component will rapidly escalate.

Eq. (4) describes the relationship between the applied load and resulting displacement of the component, highlighting the complex interplay between these factors in determining the stability and integrity of the structure under different loading conditions.

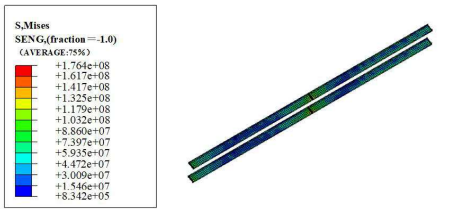

(a) Overall stress map

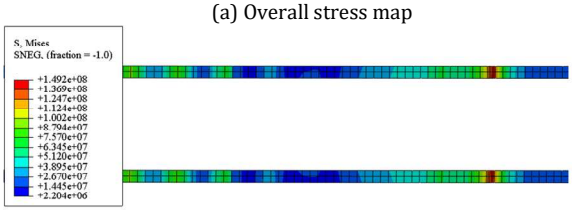

(b) Localized stress cloud at mid-span upper flange

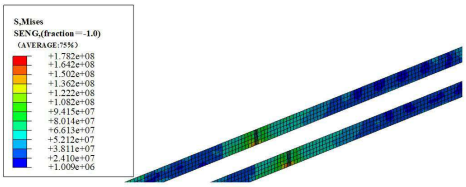

(c) Localized stress cloud in mid-span web

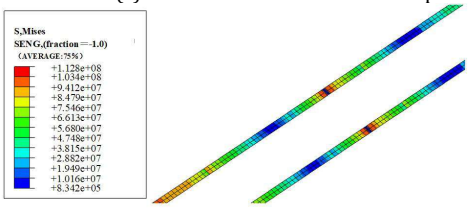

(d) Localized stress cloud at lower flange in mid-span

Fig. 9 Equivalent stress cloud of combined girder bridge under stage S13

$$[K]\{U\} = \{F\} \tag{4}$$

Using the incremental method to study the second type of stability problem, the ultimate load is divided into sufficiently small increments and gradually applied to the component. During each incremental loading period, the load-displacement relationship can be regarded as a linear relationship:

$$[K]_{i-1}\{U\}_i = \{\Delta F\}_i \tag{5}$$

When the component is loaded to the n -th increment, the total load applied to the component and the total displacement can be expressed as follows:

$$\begin{cases} \{F\}_n = \{F\}_0 + \sum_{i=1}^{n}\{\Delta F\}_i \\ \{U\}_n = \{U\}_0 + \sum_{i=1}^{n}\{\Delta U\}_i \end{cases} \begin{cases} \{F\}_n = \{F\}_0 + \sum_{i=1}^{n}\{\Delta F\}_i \\ \{U\}_n = \{U\}_0 + \sum_{i=1}^{n}\{\Delta U\}_i \end{cases} \begin{cases} \{F\}_n = \{F\}_0 + \sum_{i=1}^{n}\{\Delta F\}_i \\ \{U\}_n = \{U\}_0 + \sum_{i=1}^{n}\{\Delta U\}_i \end{cases} \tag{6}$$

Finite element software utilizes this method to solve such stability problems, calculating each load and displacement increment for elastoplastic components considering initial imperfections and geometric nonlinearity.

The steel main girder made of a high-strength thin steel plate faces a significant risk of local buckling under external loading during construction, especially when certain parts of the plate are as thin as 20 mm. Local buckling can disrupt the force distribution within the girder, thereby affecting its overall stability and stiffness. Therefore, the local stability of the girder is important in the analysis. To address this, the flexure module of ABAQUS finite element analysis software is used for local stability validation under the construction stages of S3, S6, S9, and S11. These validations will focus on identifying the fourth-order modes and accurately locating locations where local buckling may occur, enabling targeted interventions to improve the structural integrity of the girder.

Fig.10 shows the instability modals of the steel main girder under S3, S6, S9, and S11. The first-order modal instability mainly occurs in the mid-span web of span 1, especially near the upper flange. It is worth noting under stage S6, the second-order modal instability was detected corresponding to the stage of installing the second span deck slab. The characteristic of this instability is the buckling at the connection between the steel main girder and the diaphragm beam at pier 1, indicating a transverse offset buckling in this area. These local instabilities are mainly due to the insufficient stiffness of the web plate compared to the upper and lower flanges. Comprehensive analysis indicates that this lack of stiffness is the main reason for local buckling instability of the web plate. To alleviate this issue and improve overall structural stability, it is recommended to implement stiffening measures at the web plate. This will increase its resistance to buckling and ensure greater structural integrity of the girder under different loading conditions

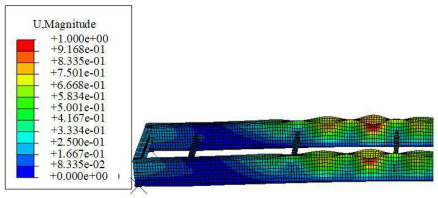

(a) The 1st order instability plot of S3

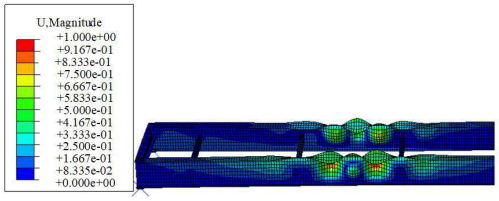

(b) The 2nd order instability diagram of S3

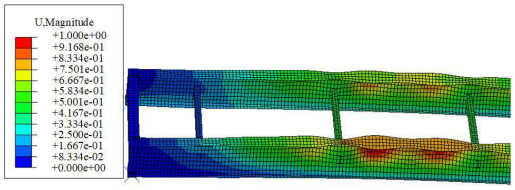

(a) The 1st order destabilization diagram of S3

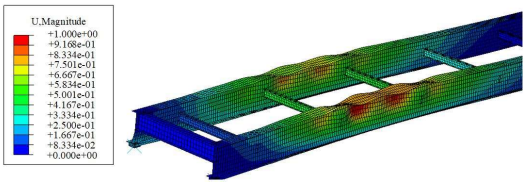

(b) The 2nd order instability map of S6

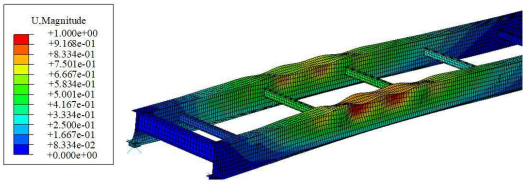

(a) The 1st order destabilization diagram of S9

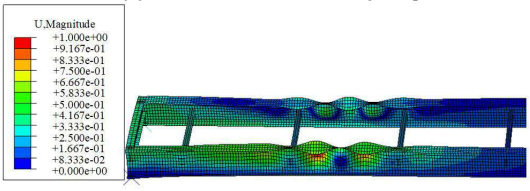

(b) The 2nd order destabilization diagram of S9

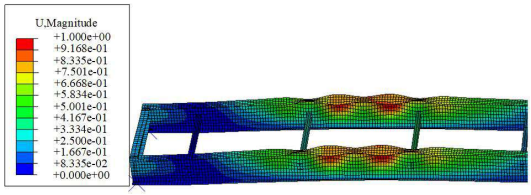

(a) The 1st order destabilization diagram of S11

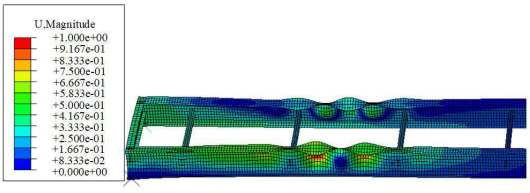

(b) The 2nd order instability diagram of S11

Fig. 10 Instability modal diagram of steel main girder under dangerous working conditions

4. Conclusion

Mechanical property and local instability analysis is conducted on a benchmark bridge to determine the most unfavorable construction conditions and the most vulnerable instability locations. This study examined the stress distribution of steel plate composite girder bridges under different construction scenarios. The main conclusions are as follows:

(1) In stages S3 (installation of the first span bridge deck) and S4 (pouring of the first span wet joint) before stage S13 (bridge deck paving and retaining wall construction), there was a significant change in the stress displacement of the double main girder steel plate beam. During the construction, pier 2, pier 4, and the center of the side span were identified as main locations. These areas experienced higher local stresses, and the center of the side span is always the position with the greatest deflection location.

(2) Under several dangerous construction conditions, the stress concentration in the double main girder steel plate composite girders is within the specified safety range. However, the stress concentration areas are mainly located in the middle of the first span of the steel main girder and around piers 2 and 4.

(3) The first-order modal instability buckling for all four conditions (S3, S6, S9, and S11) occurs at the mid-web (offside near the upper flange position) of span 1. In S6 (installation of the second span deck slab), the second-order modal instability buckling was observed at the connection between the steel main girder and diaphragm of Pier 1. The characteristic of this buckling is the lateral deflection of the upper flange web and the end transverse girder. The analysis emphasizes that compared with the upper and lower flanges, the insufficient thickness of the web plate leads to local instability. To alleviate this situation, it is recommended to strengthen the web plate at critical positions to enhance its resistance to buckling and improve the overall stability of the steel main girder.

Acknowledgments

The first author wishes to thank the National Natural Science Foundation of China for its financial support (N0.52208476, N0.52308493).

References

Bajaber, M. A., & Hakeem, I. Y., UHPC evolution, development, and utilization in construction: a review. Journal of Materials Research and Technology, vol. 10, pp. 1058-1074, 2021. https://doi.org/10.1016/j.jmrt.2020.12.051

Biscaya, A., Pedro, J. J. O., & Kuhlmann, U., Experimental behavior of longitudinally stiffened steel plate girders under combined bending, shear, and compression. Engineering Structures, vol. 238, pp. 112139, 2021. https://doi.org/10.1016/j.engstruct.2021.112139

Chithra, J., Nagarajan, P., & Sajith, A. S., Investigations in twin-cell box girder bridges subjected to combined effects of bending and torsion. Innovative Infrastructure Solutions, vol. 7, pp. 120, 2022. https://doi.org/10.1007/s41062-021-00719-2

Csillag, F., & Pavlović, M., Push-out behavior of demountable injected vs. blind-bolted connectors in FRP decks. Composite Structures, vol. 270, pp. 114043, 2021. https://doi.org/10.1016/j.compstruct.2021.114043

Ding, J., Zhu, J., Kang, J., & Wang, X., Experimental study on grouped stud shear connectors in precast steel- UHPC composite bridge. Engineering Structures, vol. 242, pp. 112479, 2021. https://doi.org/10.1016/j.engstruct.2021.112479

He, J., Suwaed, A. S., & Vasdravellis, G., Horizontal push-out tests and parametric analyses of a locking-bolt demountable shear connector. Structures, vol. 35, pp. 667-683, 2022. https://doi.org/10.1016/j.istruc.2021.11.041

He, Z. Q., Chen, J., Liu, Z., & Ma, Z.J., An Explicit Approach for Determining the Rational Length of Steel Portion in Steel-Concrete Hybrid Girder Bridges. Journal of Bridge Engineering, vol. 28, no. 1, pp. 05022011, 2023. https://doi.org/10.1061/JBENF2.BEENG-5798

Jiang, H., Fang, H., Liu, J., Fang, Z., & Zhang, J., Experimental investigation on shear performance of transverse angle shear connectors. Structures, vol. 33, pp. 2050-2060, 2021. https://doi.org/10.1016/j.istruc.2021.05.071

Jung, D. S., Park, S. H., Kim, T. H., Han, J. W., & Kim, C. Y., Demountable bolted shear connector for easy deconstruction and reconstruction of concrete slabs in steel–concrete bridges. Applied Sciences, vol. 12, no. 3, pp. 1508, 2022. https://doi.org/10.3390/app12031508

Kaplan, O., Guney, Y., & Dogangun, A., A period-height relationship for newly constructed mid-rise reinforced concrete buildings in Turkey. Engineering Structures, vol. 232, pp. 111807, 2021. https://doi.org/10.1016/j.engstruct.2020.111807

Lee, J., Kim, H., Lee, K., & Kang, Y. J., Effect of load combinations on distortional behaviors of simple-span steel box girder bridges. Metals, vol. 11, no. 8, pp. 1238, 2021. https://doi.org/10.3390/met11081238

Li, C., Lu, B., Wang, C., & Peng, W., Dynamic Performance Assessment of a Novel Hybrid Bridge System with Spread Steel Box Girders. Journal of Bridge Engineering, vol. 27, no. 1, pp. 04021097, 2022. https://doi.org/10.1061/(ASCE)BE.1943-5592.0001805

Liang, H., Li, B., Liu, Z., Tan, K., Zhang, Y., Zhang, Y., & Deng, K., Staggered-supported steel anchor box system for cable-stay bridges. Journal of Bridge Engineering, vol. 27, no. 7, pp. 04022054, 2022. https://doi.org/10.1061/(ASCE)BE.1943-5592.0001893

Rossi, A., Nicoletti, R. S., de Souza, A. S. C., & Martins, C. H., Numerical assessment of lateral distortional buckling in steel-concrete composite beams. Journal of Constructional Steel Research, vol. 172, pp. 106192, 2020. https://doi.org/10.1016/j.jcsr.2020.106192

Siwowski, T., Rajchel, M., &Wlasak, L., Experimental study on the static and dynamic performance of a novel GFRP bridge girder. Composite Structures, vol. 259, pp. 113464, 2021. https://doi.org/10.1016/j.compstruct.2020.113464

Soto, A. G., Caldentey, A. P., Peiretti, H. C., & Benítez, J. C., Experimental behavior of steel concrete composite box girders subject to bending, shear, and torsion. Engineering Structures, vol. 206, pp. 110169, 2020. https://doi.org/10.1016/j.engstruct.2020.110169

Wei, F., Luo, H.W., Liang, L.N., Xiao, Y.B., Su, C., Mechanical Performance Analysis of Steel-Concrete Joint Section of a Long-Span Hybrid Girder Cable-Stayed Bridge Based on Field Test. Journal of Chang'an University (Natural Science Edition), vol. 41, no. 5, pp. 54-65, 2021. https://DOI: 10.19721/j.cnki.1671-8879.2021.05.006

Xu, C., Zhang, L., Su, Q., & Abbas, S., Mechanical behavior of a novel steel-concrete joint in concrete-composited hybrid continuous bridges. Structures, vol. 36, pp. 291-302, 2022. https://doi.org/10.1016/j.istruc.2021.12.030

Zhou, Y., Pei, Y., Zhou, Y., Hwang, H. J., & Yi, W., Field measurements for calibration of simplified models of the stiffening effect of infill masonry walls in high-rise RC framed and shear-wall buildings. Earthquake Engineering and Engineering Vibration, vol. 19, pp. 87-104, 2020. https://doi.org/10.1007/s11803-020-0549-y

Disclaimer